Inorganic Chemistry

Article

pubs.acs.org/IC

Gold(III) Porphyrins Containing Two, Three, or Four β,β′-Fused Quinoxalines. Synthesis, Electrochemistry, and Effect of Structure and Acidity on Electroreduction Mechanism

Zhongping Ou,*[,†,‡] Tony Khoury,[§] Yuanyuan Fang,[†,‡] Weihua Zhu,[†,‡] Paul J. Sintic,[§] Maxwell J. Crossley,*[,§] and Karl M. Kadish*[,‡]

[†]School of Chemistry and Chemical Engineering, Jiangsu University, Zhenjiang 212013, China

[‡]Department of Chemistry, University of Houston, Houston, Texas 77204-5003, United States

[§]School of Chemistry, The University of Sydney, NSW 2006, Australia

Supporting Information

ABSTRACT: Gold(III) porphyrins containing two, three, or four β,β′-fused quinoxalines were synthesized and examined as to their electrochemical properties in tetrahydrofuran (THF), pyridine, CH_2Cl_2, and CH_2Cl_2 containing added acid in the form of trifluoroacetic acid (TFA). The investigated porphyrins are represented as $Au(PQ_2)PF_6$, $Au(PQ_3)PF_6$, and $Au(PQ_4)PF_6$, where P is the dianion of the 5,10,15,20-tetrakis(3,5-di-*tert*-butylphenyl)porphyrin and Q is a quinoxaline group fused to a β,β′-pyrrolic position of the porphyrin macrocycle. In the absence of added acid, all three gold(III) porphyrins undergo a reversible one-electron oxidation and several reductions. The first reduction is characterized as a Au^{III}/Au^{II} process which is followed by additional porphyrin- and quinoxaline-centered redox reactions at more negative potentials. However, when 3−5 equivalents of acid are added to the CH_2Cl_2 solution, the initial Au^{III}/Au^{II} process is followed by a series of internal electron transfers and protonations, leading ultimately to triply reduced and doubly protonated $Au^{II}(PQ_2H_2)$ in the case of $Au^{III}(PQ_2)^+$, quadruply reduced and triply protonated $Au^{II}(PQ_3H_3)$ in the case of $Au^{III}(PQ_3)^+$, and $Au^{II}(PQ_4H_4)$ after addition of five electrons and four protons in the case of $Au^{III}(PQ_4)^+$. Under these solution conditions, the initial $Au(PQ_2)PF_6$ compound is shown to undergo a total of three Au^{III}/Au^{II} processes while $Au(PQ_3)PF_6$ and $Au(PQ_4)PF_6$ exhibit four and five metal-centered one-electron reductions, respectively, prior to the occurrence of additional reductions at the conjugated macrocycle and fused quinoxaline rings. Each redox reaction was monitored by cyclic voltammetry and thin-layer spectroelectrochemistry, and an overall mechanism for reduction in nonaqueous media with and without added acid is proposed. The effect of the number of Q groups on half-wave potentials for reduction and UV−visible spectra of the electroreduced species are analyzed using linear free energy relationships.

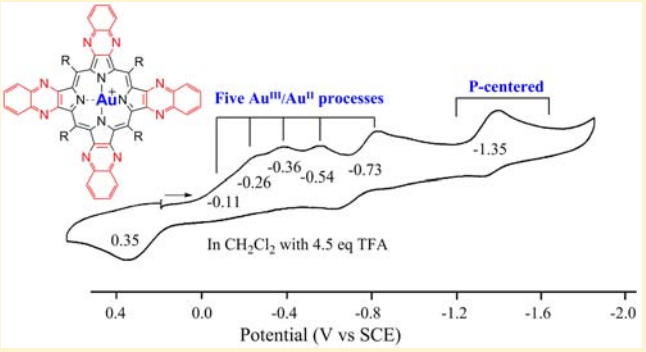

INTRODUCTION

The electroreduction of quinoxalinoporphyrins can involve the central metal ion, the conjugated porphyrin macrocycle, or the fused quinoxaline group(s), depending upon the specific compound and the experimental conditions.[1−8] The measured redox potentials will depend in each case upon the site of electron transfer, the type and oxidation state of the central metal ion, the number of fused quinoxaline groups, the specific electron-donating or electron-withdrawing substituents on the macrocycle,[3,4,6−8] and the type and number of axial ligands.[9] Protonation of the quinoxaline nitrogen atoms can also have a significant effect on the electrochemical behavior of these compounds as was demonstrated for derivatives containing both electrochemically inert Sn(IV), Cu(II), or Ni(II) central metal ions[7] and redox active central metal ions such as Co(II),[4] Mn(III),[10] Ag(III),[11] and Au(III).[12]

A positive linear shift in reduction potentials with increase in the number of fused quinoxaline (Q) groups has been well-documented upon going from simple metalloporphyrins to derivatives of mono- and "linear" bis-quinoxalinoporphyrins, with the magnitude of the shift depending upon the type and oxidation state of the central metal ion and the specific site of electron transfer.[3−8,11−16] A much smaller shift in macrocycle-centered reduction potentials was reported upon going from the PQ to corner PQ_2 quinoxalinoporphyrins with redox inactive centers,[13] but it was not known if the same trend would be observed for metal-centered reactions, nor was it known how the addition of three or four Q groups to the gold(III) porphyrins would be reflected in $E_{1/2}$ values for the multiple reductions of these compounds in nonaqueous media. This is

Received: October 31, 2012
Published: February 20, 2013

   dx.doi.org/10.1021/ic302380z | *Inorg. Chem.* 2013, 52, 2474−2483

Chart 1. Structures of Gold(III) Quinoxalinoporphyrins

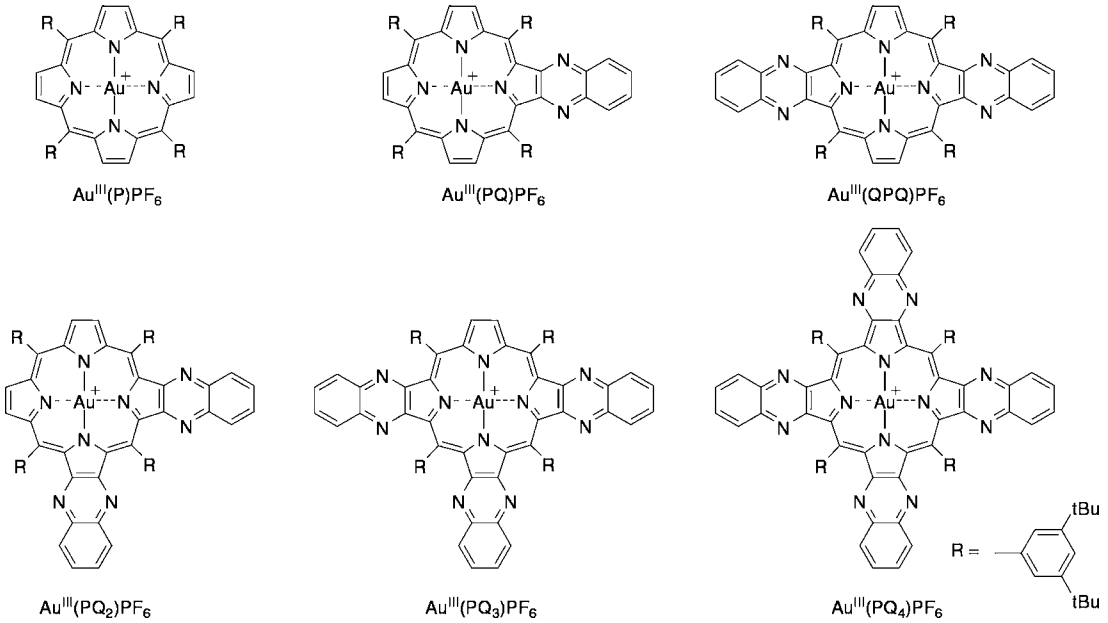

Scheme 1. Published Mechanism for the Reduction of $Au^{III}(PQ)^+$ in Non-Aqueous Media Containing TFA[12]

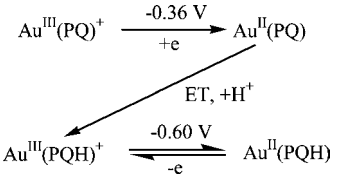

investigated in the present study for three newly synthesized gold(III) porphyrins which are represented as $Au(PQ_2)PF_6$, $Au(PQ_3)PF_6$, and $Au(PQ_4)PF_6$, where P is the dianion of the 5,10,15,20-tetrakis(3,5-di-*tert*-butylphenyl)porphyrin and Q is a quinoxaline group fused to the β,β'-pyrrolic positions of the porphyrin macrocycle (Chart 1).

Gold(III) quinoxalinoporphyrins have attracted a great deal of interest, in part because they are easy to reduce and can undergo multiple electron additions.[2−4,6,7] The first reduction involves an Au^{III}/Au^{II} conversion in all cases while the second and third one-electron reductions are proposed to be porphyrin ring-centered electron transfers. Further reductions are also possible at the fused quinoxaline group(s) and are often observed at more negative potentials.[5,17] Gold(III) quinoxalinoporphyrins are also of interest since the mono- and bis-quinoxaline derivatives were recently shown to undergo multiple Au^{III}/Au^{II} process in acidic solutions of CH_2Cl_2 or PhCN,[12] as shown in Scheme 1 for the case of $Au(PQ)PF_6$.

Table 1. Half-Wave Potentials (V vs SCE) of $Au^{III}(PQ_n)$ PF_6 (n = 0−4) in CH_2Cl_2, Pyridine, and THF, 0.1 M TBAP

		oxidation	reduction					potential separation ($\Delta E_{1/2}$,V)			
solvent	cpd	first	first	second	third	fourth	fifth	1red-2red	2red-3red	1ox-1red	ref
CH_2Cl_2	P	1.59	−0.64	−1.15				0.51		2.23	3, 12
	PQ	1.54	−0.47	−0.97	−1.82[a]			0.50	0.85	2.01	3, 12
	QPQ	1.48	−0.26	−0.84	−1.64[a]			0.58	0.80	1.74	12
	PQ_2	1.48	−0.31	−1.05	−1.55[a]	−1.82[a]		0.74	0.50	1.79	*tw*
	PQ_3	1.36	−0.17	−0.90	−1.50	−1.66		0.73	0.60	1.53	*tw*
	PQ_4	1.24	−0.06	−0.97	−1.39	−1.53	−1.66	0.91	0.42	1.30	*tw*
Pyridine	P		−0.52	−1.08	−1.76			0.56	0.68		2
	PQ		−0.35	−0.87	−1.69			0.52	0.82		3
	QPQ		−0.17	−0.71	−1.56			0.54	0.85		*tw*
	PQ_2		−0.24	−0.97	−1.48	−1.85[a]		0.73	0.51		*tw*
	PQ_3		−0.11	−0.82	−1.44	−1.68[a]	−1.97[a]	0.71	0.60		*tw*
	PQ_4		−0.01	−0.86	−1.32	−1.76[b]	−1.76[b]	0.85	0.46		*tw*
THF[c]	P	1.89[a]	−0.40	−1.10	−1.77			0.70	0.67	2.29	2
	PQ	1.77[a]	−0.20	−0.88	−1.65	−2.22[a]		0.68	0.77	1.97	3
	QPQ	1.60[a]	−0.02	−0.70	−1.53	−2.04[a]	−2.22[a]	0.68	0.83	1.62	*tw*
	PQ_2	1.53	−0.07	−0.95	−1.45	−1.97[a]	−2.26[a]	0.88	0.50	1.61	*tw*
	PQ_3	1.45	0.09	−0.76	−1.37	−1.85[a]	−2.05[a]	0.85	0.61	1.54	*tw*
	PQ_4	1.32	0.17	−0.80	−1.28	−1.79[a]	−2.01[a]	0.97	0.48	1.49	*tw*

[a]Irreversible peak potential at a scan rate of 0.10 V/s. *tw* = this work. [b]Two overlapping one-electron reductions. [c]Potentials vs Ag/AgCl.

dx.doi.org/10.1021/ic302380z | *Inorg. Chem.* 2013, 52, 2474−2483

To determine if additional proton induced metal-centered reductions might occur with further increase in the number of Q groups, the three newly synthesized compounds were therefore examined not only as to their electrochemical properties in tetrahydrofuran (THF), pyridine, and CH_2Cl_2 but also in CH_2Cl_2 containing added acid in the form of trifluoroacetic acid (TFA). The effect of the number of Q groups on the redox potentials and protonation reactions is discussed, and an overall reduction/oxidation mechanism is then proposed. For simplification, the examined Au(III) porphyrins are represented in the manuscript as $Au(PQ_2)^+$, $Au(PQ_3)^+$, and $Au(PQ_4)^+$.

RESULTS AND DISCUSSION

Electrochemistry of $Au^{III}(PQ_2)PF_6$, $Au^{III}(PQ_3)PF_6$, and $Au^{III}(PQ_4)PF_6$. The electrochemistry of $Au(PQ_2)^+$, $Au(PQ_3)^+$, and $Au(PQ_4)^+$ was initially carried out in CH_2Cl_2, pyridine, and THF containing 0.1 M TBAP as supporting electrolyte. The half-wave potentials are summarized in Table 1 which also includes data for previously investigated gold(III) porphyrins having zero, one, or two linear β,β'-fused quinoxaline groups on the macrocycle.[2,3,12] Cyclic voltammograms of the six $Au^{III}(PQ_n)PF_6$ complexes analyzed in the present study are illustrated in Figure 1 for the reductions in CH_2Cl_2 containing 0.1 M TBAP. As seen in the figure, and also previously reported,[12] $Au^{III}(P)^+$, $Au^{III}(PQ)^+$, and $Au^{III}(QPQ)^+$ undergo two or three one-electron reductions in CH_2Cl_2 (Figure 1a), while four or five reductions are observed for $Au^{III}(PQ_2)^+$, $Au(PQ_3)^+$, and $Au^{III}(PQ_4)^+$ under the same solution conditions (Figure 1b).

The first one-electron reduction of $Au^{III}(PQ_n)^+$ is metal-centered,[3,12] and this was verified by electron spin resonance (ESR) in the present study for the product of singly reduced $Au^{III}(PQ_3)^+$ and $Au^{III}(PQ_4)^+$ which show typical Au(II) signals at $g = 2.06$ (Supporting Information, Figure S1). The reversible half wave potentials for the Au^{III}/Au^{II} process range from −0.64 to 0.17 V depending upon the solvent (CH_2Cl_2, Py, or THF) and number of Q groups (0 to 4) fused to the macrocycle (see Table 1). The first oxidation of the six $Au^{III}(PQ_n)^+$ complexes is reversible in CH_2Cl_2 and involves a one-electron abstraction from the conjugated π-ring system, with $E_{1/2}$ values ranging from 1.59 to 1.24 V (see Table 1). The absolute potential difference between the reversible first reduction of the six Au(III) porphyrins at the central metal ion and the reversible first oxidation at the conjugated macrocycle ($\Delta E_{1/2}$) range from 2.23 to 1.30 V in CH_2Cl_2 and is smallest in the case of $Au(PQ_3)^+$ (1.53 V) and $Au(PQ_4)^+$ (1.30 V). This separation is solvent dependent, as seen by the data in THF, where reversible oxidations are seen only for the PQ_2, PQ_3, and PQ_4 derivatives, leading to $\Delta E_{1/2}$ values of 1.61, 1.54, and 1.49, respectively.

The second and third reversible reductions of $Au(P)^+$, $Au(PQ)^+$, and $Au(QPQ)^+$ have been shown to occur at the conjugated π-ring system to give Au^{II} π-anion radical and dianions under all solution conditions. The potential difference between the Au^{III}/Au^{II} process and the first ring-centered reduction of the three newly synthesized quinoxalinoporphyrins depends slightly upon solvent, with measured $\Delta E_{1/2}$ values ranging from 0.50 to 0.58 V in CH_2Cl_2 or pyridine and from 0.68 to 0.70 V in THF. Much larger potential separations are seen between the second and the third one-electron reductions of $Au(PQ)^+$ and $Au(QPQ)^+$ in the above listed solvents where the $\Delta E_{1/2}$ values range from 0.77 to 0.85 V (see Figure 1 and

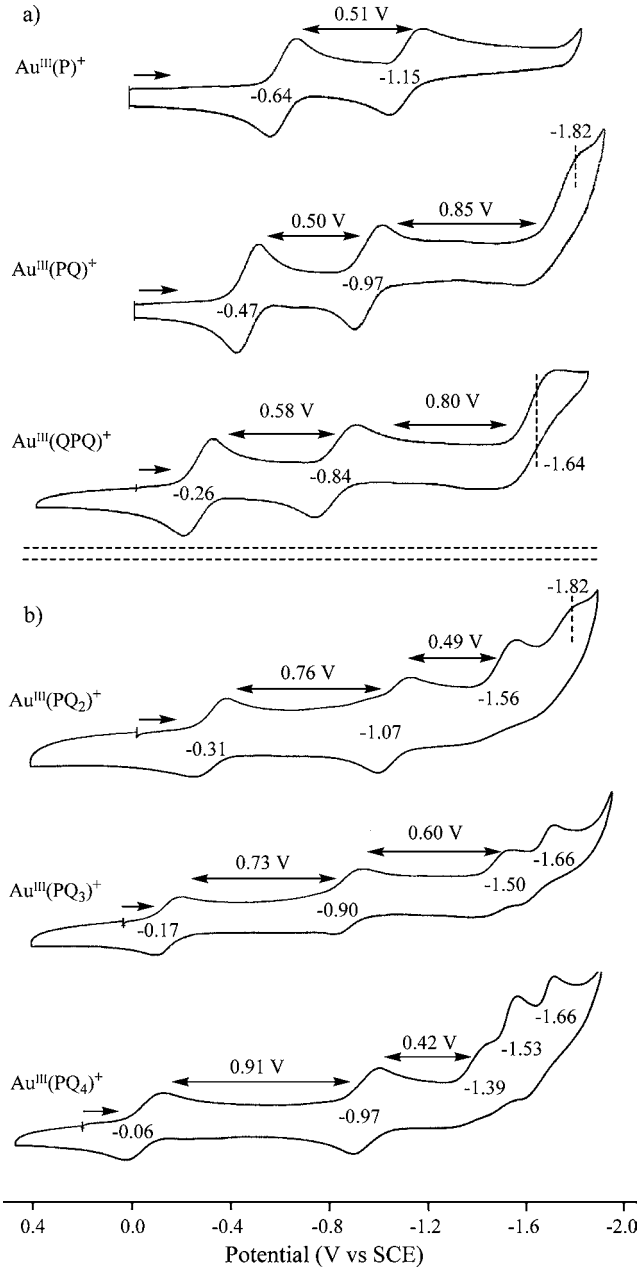

Figure 1. Cyclic voltammograms of Au(III) quinoxalinoporphyrins which undergo (a) 2−3 reductions and (b) 4−5 reductions in CH_2Cl_2 containing 0.1 M TBAP.

Table 1). This unusually large potential separation between formation of the Au(II) porphyrin π-anion radical and dianion contrasts markedly with what is known to occur for ring-centered reductions of all other metalloporphyrins with M(II) centered metals, where $\Delta E_{1/2}$ values of 0.4 to 0.5 V are generally observed.[1] This might at first suggest a different site of electron transfer in the case of the PQ and QPQ derivatives, but the situation becomes more complex when also analyzing potentials for the first three reductions and first oxidation of the PQ_2, PQ_3, and PQ_4 compounds. This analysis is given in Figure 2 where correlations between half-wave potentials ($E_{1/2}$) and n, the number of Q groups, are presented. As seen in the figure, the first and third reductions of $Au^{III}(PQ_n)^+$ shift positively in potential by 0.14 to 0.15 V per added Q group (an easier reduction) upon going from $n = 0$ to $n = 4$ while the first

dx.doi.org/10.1021/ic302380z | Inorg. Chem. 2013, 52, 2474−2483

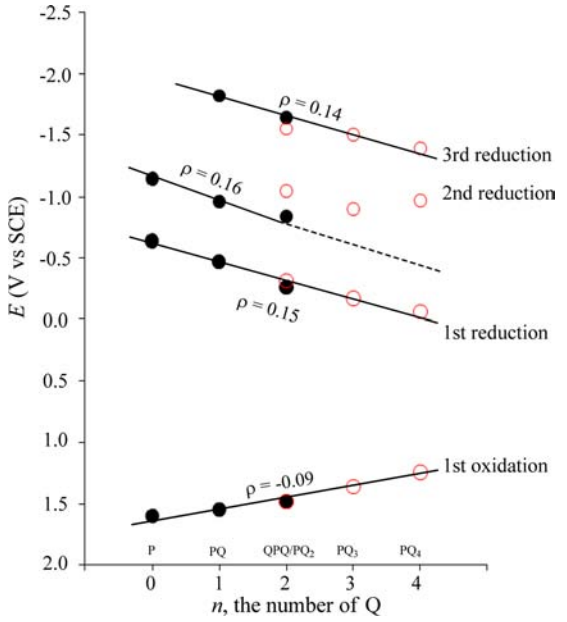

Figure 2. Plots of redox potentials of $Au^{III}(PQ_n)^+$ in CH_2Cl_2 vs the number of quinoxaline groups, where the black filled circles represent of P, PQ, and QPQ and the red open circles represent PQ_2, PQ_3, and PQ_4.

Scheme 2. Proposed Mechanism for First Three Reductions of $Au^{III}(PQ_2)^+$, $Au^{III}(PQ_3)^+$, and $Au^{III}(PQ_4)^+$ in CH_2Cl_2

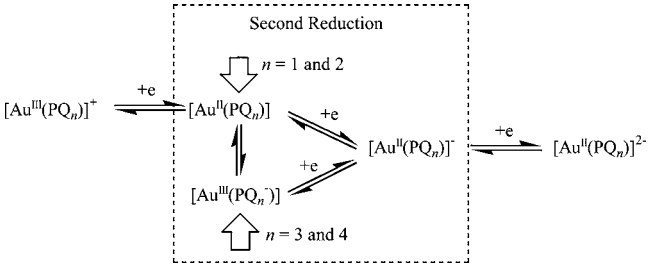

oxidation shifts negatively by 0.09 V with the change in structure, that is, an easier oxidation occurs as the number of fused Q groups on the molecule is increased.

Changes in the measured $E_{1/2}$ values for oxidation and reduction of a given compound in the $Au^{III}(PQ_n)^+$ series upon going from $Au^{III}(P)^+$ to $Au^{III}(PQ_4)^+$ will depend upon a number of factors, the most important of which are substituent effects of the fused Q groups on the electroreduction or electrooxidation site, changes in the size of the conjugated π-system, and changes in planarity of the macrocycle with increase in number of Q groups or change of solvent. A progressively easier reduction would be expected to occur upon increasing the number of electron-withdrawing Q groups, and an easier reduction would also be expected to occur if the size of the conjugated π-system were increased upon going from $Au^{III}(P)^+$ to $Au^{III}(PQ_4)^+$. In the case of oxidation, a harder electron abstraction process (more positive potential) would be expected with increase in electron-withdrawing effect of the Q substituents but an easier oxidation would result with an increase in size of the porphyrin π-ring system. An increased nonplanarity of the porphyrin macrocycle might also lead to an easier oxidation as has been demonstrated for a number of compounds.[1,18−21]

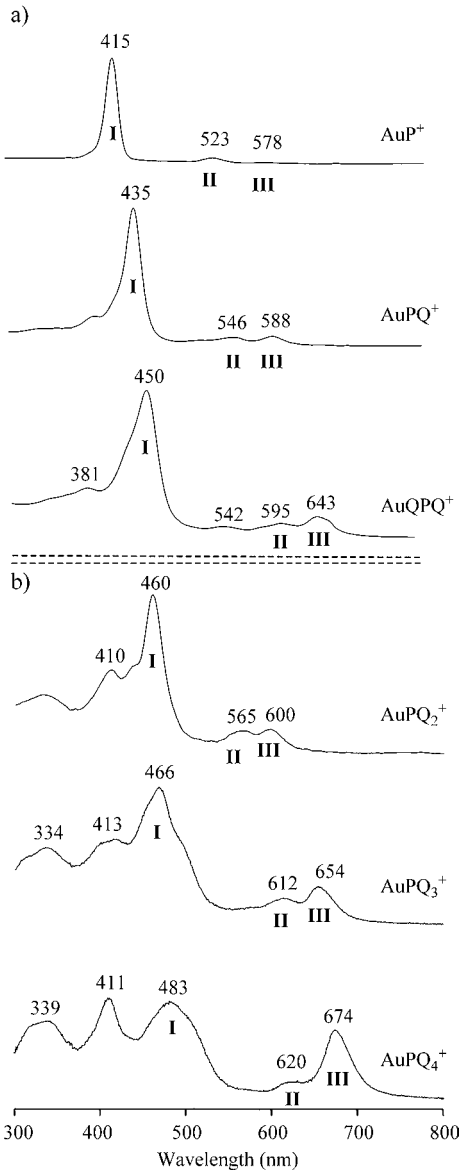

Figure 3. UV−visible spectra of (a) $Au^{III}(P)^+$, $Au^{III}(PQ)^+$, $Au^{III}(QPQ)^+$ and (b)$Au^{III}(PQ_2)^+$, $Au^{III}(PQ_3)^+$, and $Au^{III}(PQ_4)^+$ in CH_2Cl_2, 0.1 M TBAP.

The shift of $E_{1/2}$ with increase in number of Q groups for the second reduction of $Au^{III}(PQ_n)^+$ to form an Au^{II} π-anion radical is a combination of two trends. The first involves the P, PQ, and QPQ derivatives (solid points in Figure 2) where half-wave potentials linearly shift in a positive direction with increase in Q (slope = 0.16 V) while the second involves $Au^{III}(PQ_2)^+$, $Au^{III}(PQ_3)^+$, and $Au^{III}(PQ_4)^+$ (open points in Figure 2) where there is little to no significant shift in $E_{1/2}$. This suggests a change in mechanism or change in charge delocalization between the two series of compounds. Interestingly, the separation in $E_{1/2}$ between the first and third reductions of $Au^{III}(PQ_n)^+$ complexes remains relatively constant at 1.33 to 1.38 V for all of the compounds except PQ_2 which displays a smaller separation of 1.24 V in CH_2Cl_2.

This relatively constant potential separation between the first and third reductions further emphasizes the unexpected trends in $E_{1/2}$ for the second reduction as a function of the number of Q groups on the macrocycle. As seen in Figures 1 and 2, the

dx.doi.org/10.1021/ic302380z | Inorg. Chem. 2013, 52, 2474−2483

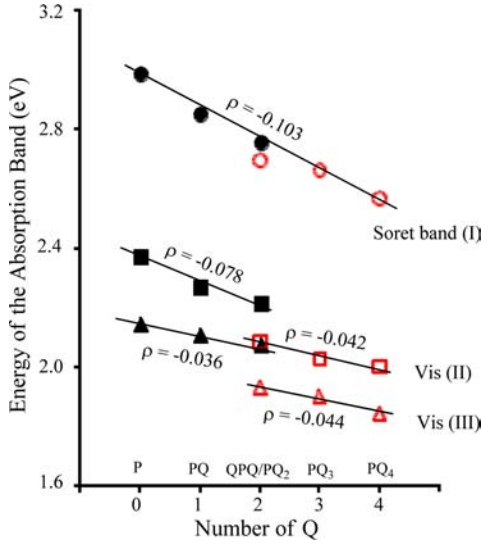

Figure 4. Plots of energy for the Soret and two visible bands of $Au^{III}(PQ_n)^+$ vs the number of Q groups on the macrocycle for P, PQ_2 and QPQ (black solid points) and PQ_2, PQ_3, and PQ_4 (red open points).

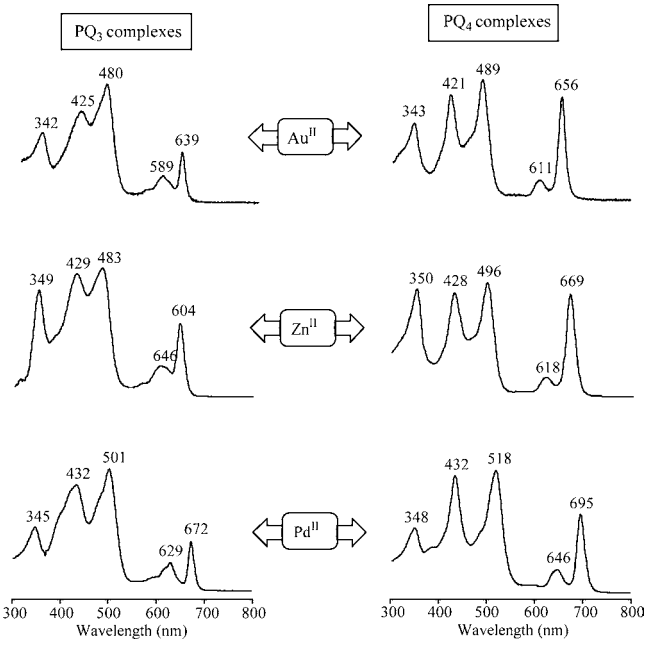

Figure 6. Comparisons of the UV–visible spectra of $Au^{II}(PQ_n)$, $Zn^{II}(PQ_n)$, and $Pd^{II}(PQ_n)$ (n = 3 and 4) in CH_2Cl_2 containing 0.1 M TBAP.

second macrocycle-centered reduction of $Au^{II}(PQ_2)^+$, $Au^{III}(PQ_3)^+$, and $Au^{III}(PQ_4)^+$ become increasingly more difficult as compared to the first reduction, the absolute difference in potential between these two processes being 910 mV for $Au^{III}(PQ_4)^+$ as compared to 500 mV for the same two electron transfer reactions of $Au^{III}(PQ)^+$. This result is consistent with an increased negative charge being located on the macrocycle after the first metal-centered reduction of $Au^{II}(PQ_2)^+$, $Au^{III}(PQ_3)^+$, and $Au^{III}(PQ_4)^+$ and might be accounted by a transfer of charge between the Au(II) central metal ion and the porphyrin macrocycle as shown in Scheme 2.

In contrast to the second reduction, a linear relationship is observed in the plot of $E_{1/2}$ vs the number of β,β'-fused Q substituents for all other reactions of $Au^{III}(PQ_n)^+$ (Figure 2). Similar relationships between $E_{1/2}$ and n are also seen for reductions and oxidations of the $Au^{III}(PQ_n)^+$ complexes in pyridine and THF (Supporting Information, Figure S2), thus indicating that there is little to no solvent effect on the potential shifts.

Spectra of Neutral and Reduced Compounds. UV–visible spectra of the different $Au^{III}(PQ_n)^+$ compounds in CH_2Cl_2 are shown in Figure 3. The P, PQ_2 and QPQ derivatives (Figure 3a) are each characterized by a single sharp Soret band at 415, 435, and 450 nm, respectively, while the PQ_2, PQ_3, and PQ_4 derivatives (Figure 3b) display three relatively broad Soret bands as seen in the figure. The energy of the most intense Soret band, labeled as I in Figure 3, and that of the two visible bands, labeled as II and III, all shift toward longer wavelengths as a function of the number of Q groups on $Au^{III}(PQ_n)^+$. This relationship is shown in Figure 4 where a plot of Soret band energy vs the number of Q groups shows one linear relationship for all six compounds and that of the two

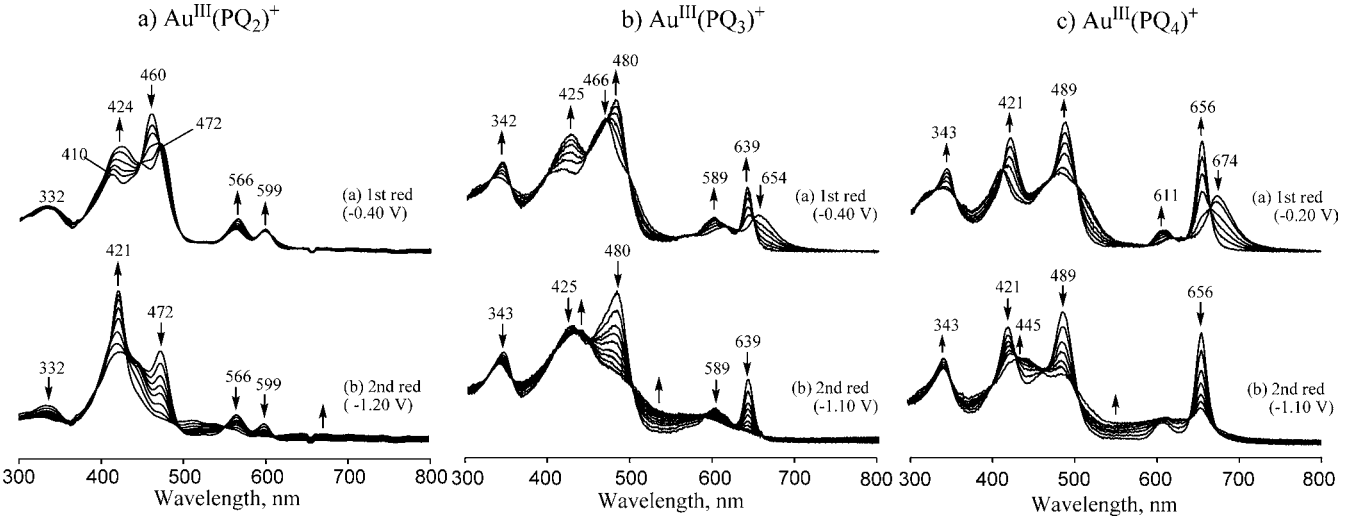

Figure 5. Thin-layer UV–visible spectral changes of $Au^{III}(PQ_2)PF_6$, $Au^{III}(PQ_3)PF_6$, and $Au^{III}(PQ_4)PF_6$ in CH_2Cl_2 containing 0.1 M TBAP during the reductions at the indicated potential.

dx.doi.org/10.1021/ic302380z | Inorg. Chem. 2013, 52, 2474–2483

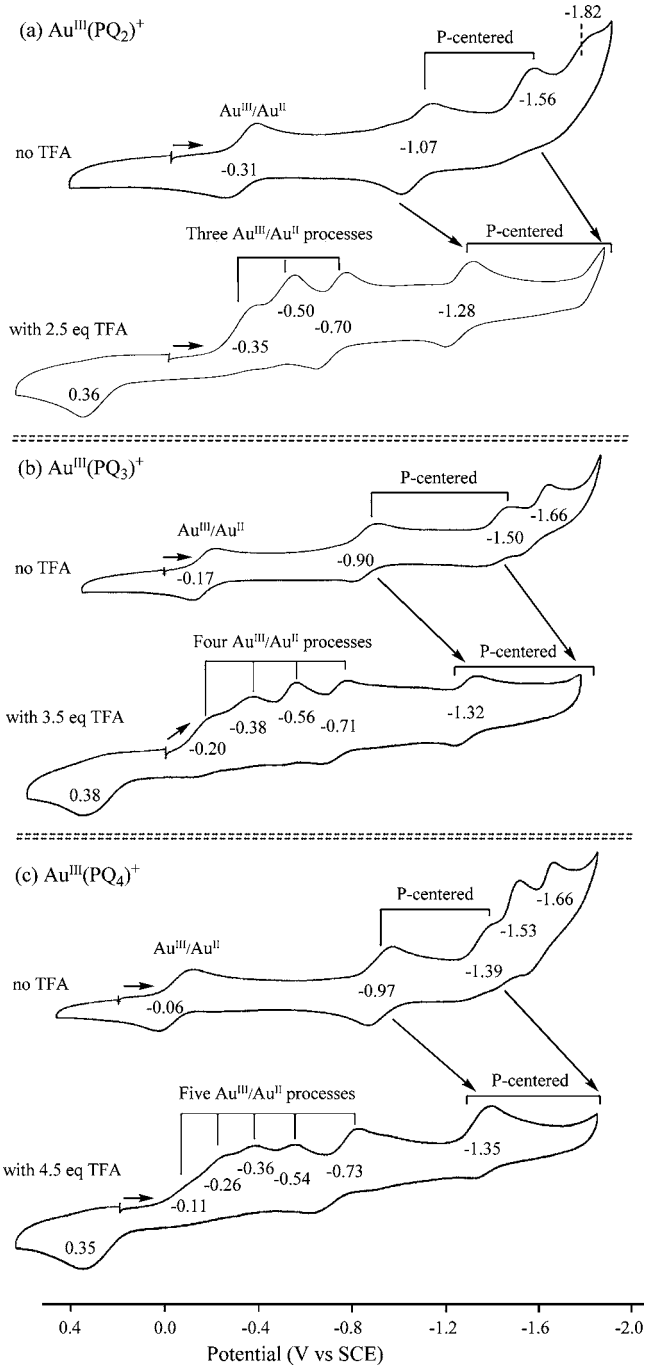

Figure 7. Cyclic voltammograms of (a) $Au^{III}(PQ_2)^+$, (b) $Au^{III}(PQ_3)^+$, and (c) $Au^{III}(PQ_4)^+$ in CH_2Cl_2 containing 0.1 M TBAP in the absence and presence of 2.5, 3.5, or 4.5 equiv of added TFA.

visible band shows two linear relationships, one for P, PQ, and PQ_2 and the other for PQ_2, PQ_3, and PQ_4 (Figure 4).

To evaluate possible changes in the site of electron transfer with increasing number of Q groups, the electrode reactions of $Au^{III}(PQ_2)^+$, $Au^{III}(PQ_3)^+$, and $Au^{III}(PQ_4)^+$ were monitored in CH_2Cl_2, 0.1 M TBAP by UV–visible spectroelectrochemistry. Spectral changes obtained during the first two reductions of these three compounds are shown in Figure 5.

Similar evolutions in UV–visible spectra are seen during the first metal-centered reduction of the three porphyrins in CH_2Cl_2. For example, the three Soret bands of neutral $Au^{III}(PQ_4)^+$ are red-shifted by 4–10 nm as the Au(II) complex is formed (Figure 5c) while the visible bands are blue-shifted by 9–18 nm during this one-electron addition process. The three Soret bands of $Au^{III}(PQ_3)^+$ are also red-shifted by 5–13 nm while the Q bands exhibit a 14–23 nm blue-shift during the first controlled potential reduction at −0.20 V (Figure 5b). Several isosbestic points are seen, indicating the lack of spectrally detectable intermediates in the Au^{III}/Au^{II} transition. The final spectra of singly reduced $Au^{III}(PQ_3)^+$ and $Au^{III}(PQ_4)^+$ are similar in CH_2Cl_2 to that of unreduced Pd^{II} and Zn^{II} quinoxalinoporphyrins containing the same number of Q groups. This comparison is shown in Figure 6 and further confirms the formation of gold(II) porphyrins after a one-electron reduction of the neutral compound.

The second and third reductions of $Au^{III}(PQ_n)^+$ are proposed to occur at the porphyrin π-ring system, and the decreased intensity of the Soret bands in the final spectra after reduction are consistent with this assignment. Examples of the spectral changes during the conversion of $Au^{II}(PQ_n)^+$ to its π-anion radical form are shown in Figure 5 for derivatives of PQ_2, PQ_3, and PQ_4.

Electrochemistry of $Au^{III}(PQ_2)PF_6$, $Au^{III}(PQ_3)PF_6$, and $Au^{III}(PQ_4)PF_6$ in the Presence of Acid. The electrochemistry of $Au^{III}(PQ_2)^+$, $Au^{III}(PQ_3)^+$, and $Au^{III}(PQ_4)^+$ was also carried out in CH_2Cl_2 containing H^+ in the form of TFA. Examples of cyclic voltammograms are shown in Figure 7 and illustrate the significant differences in electrochemistry which result after the addition of TFA to solution. For all three quinoxalinoporphyrins, the first Au^{III}/Au^{II} reduction (at $E_{1/2}$ = −0.31, −0.17, or −0.06 V in the absence of acid) becomes irreversible, and this process is followed at more negative potential by additional irreversible metal-centered reductions as was previously reported for $Au^{III}(PQ)^+$ and $Au^{III}(QPQ)^+$ in acidic nonaqueous media.[12] $Au^{III}(PQ_2)^+$ undergoes two irreversible reductions followed by a reversible $Au^{III/II}$ process at a scan rate of 0.1 V/s while $Au^{III}(PQ_3)^+$ and $Au^{III}(PQ_4)^+$ undergo three and four irreversible redox processes, respectively, followed at more negative potentials by a reversible Au^{III}/Au^{II} transition. The sequential irreversible reductions are all assigned as Au(III)-centered electron transfers as shown in Scheme 3.

The potentials for each reduction of the quinoxalinoporphyrins in acidic CH_2Cl_2 are given in Schemes 1 and 3 and also summarized in Table 2 for three series of compounds, $Au^{III}(PQ_n)^+$, $Au^{III}(PQ_nH_n)^+$, and $Au^{II}(PQ_nH_n)$. The first series of compounds are unprotonated, and the last two are fully protonated.

Several key points are evident from the data in Table 2, the most important of which is that the reversible potentials for reduction of the fully protonated Au(III) quinoxalinoporphyrins to their Au(II) forms are virtually independent of the number of Q groups where $E_{1/2}$ varies over the narrow range of −0.70 to −0.73 V for the PQ_n derivatives with n = 2, 3, or 4 (see also last reaction in lower part of Scheme 3).

Similar reduction potentials are also seen for reduction of the partially protonated compounds in the PQ_2, PQ_3, and PQ_4 series. For example, reduction of the mono-Q protonated compound, $Au(PQ_3H)^+$, is located at E_{pc} = −0.38 V while an almost identical potential (E_{pc} = −0.36 V) is seen for the reduction of $Au(PQ_4H_2)^+$. Similar reduction potentials are also seen for $Au^{II}(PQ_2H)$ (−0.50 V), $Au(PQ_3H_2)^+$ (−0.56 V), and $Au(PQ_4H_3)^+$ (−0.54 V).

Finally, the potential for reduction of the fully protonated Au^{II} derivatives of PQ_2, PQ_3, and PQ_4 ranges from −1.28 V for $Au^{II}(PQ_2H_2)$ to −1.35 V for $Au^{II}(PQ_4H_4)$ and varies only

dx.doi.org/10.1021/ic302380z | Inorg. Chem. 2013, 52, 2474–2483

Scheme 3. Proposed Reduction/Oxidation Mechanism of $Au(PQ_2)^+$, $Au(PQ_3)^+$, and $Au^{III}(PQ_4)^+$ in CH_2Cl_2 Containing 2.5, 3.5, or 4.5 equiv of TFA

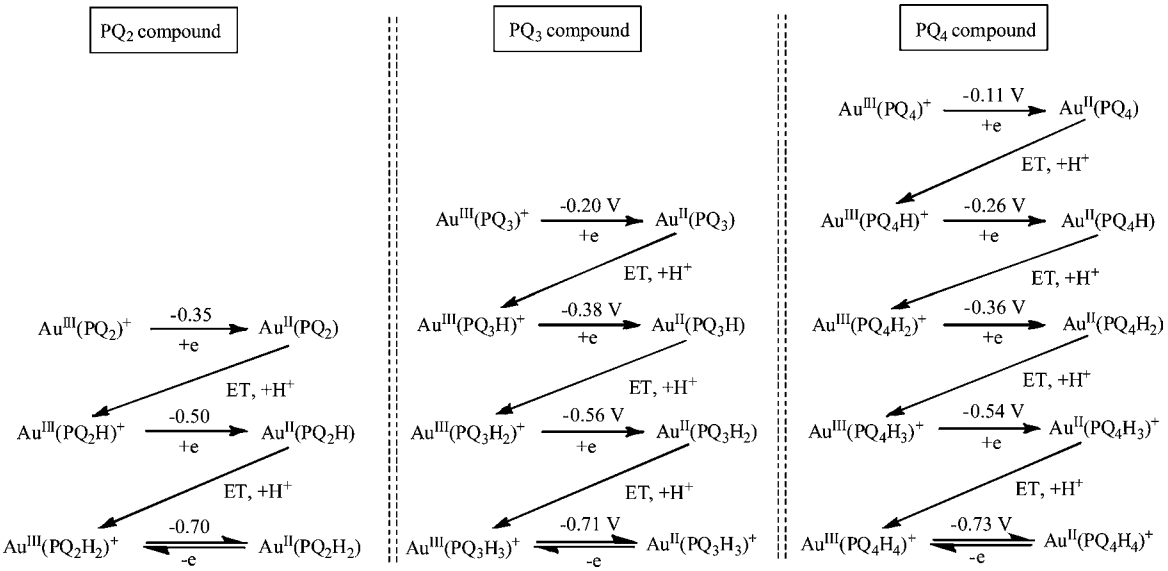

Table 2. Reduction Potentials (V vs SCE) of $Au^{III}(PQ_n)^+$, $Au^{III}(PQ_nH_n)^+$, and $Au^{II}(PQ_nH_n)$ in CH_2Cl_2, 0.1 M TBAP with added TFA[a]

	unprotonated	fully protonated		
number of Q	$Au^{III}(PQ_n)^+$	$Au^{III}(PQ_nH_n)^+$	$Au^{II}(PQ_nH_n)$	reference
0	−0.64	−0.64	−1.15	12
1	−0.36[b]	−0.60	−1.11	12
2[c]	−0.29[b]	−0.72	−1.19	12
2[d]	−0.31	−0.70	−1.28	*tw*
3	−0.20	−0.71	−1.32	*tw*
4	−0.11	−0.73	−1.35	*tw*

[a] 1.5, 2.5, 2.5, 3.5, 4.5 equiv of TFA added in solution for compounds with n = 1−4, respectively; potentials for PQ compound measured in PhCN. [b] Irreversible peak potential at a scan rate of 0.10 V/s. *tw* = this work. [c] The QPQ derivative. [d] The PQ_2 derivative.

slightly as a function of the number of Q groups on the compounds. (see Figure 7)

Spectroelectrochemistry of $Au^{III}(PQ_2)^+$, $Au^{III}(PQ_3)^+$, and $Au^{III}(PQ_4)^+$ in the Presence of TFA. Thin-layer UV−visible spectroelectrochemistry was carried out in CH_2Cl_2 containing 0.1 M TBAP and added TFA to elucidate UV−visible spectra of the PQ_2, PQ_3, and PQ_4 derivatives in each stepwise reduced and protonated forms. Spectral changes obtained during the multiple one-electron reductions of $Au^{III}(PQ_2)^+$ and $Au^{III}(PQ_3)^+$ are shown in Figures 8 and 9, and the final UV−visible spectrum after each one electron reduction of $Au^{III}(PQ_4)^+$ are shown in Figure 10. The reactants and products of the Au^{III}/Au^{II} processes are given in Scheme 3.

The unreduced Au(III) quinoxalinoporphyrins are unprotonated in CH_2Cl_2 solutions containing less than 20 equiv of added acid as evidenced by the UV−visible spectra. In contrast, protonation readily occurs for the electroreduced species, and this leads to characteristic shifts in the UV−vis spectra. For example, after potential reduction of $Au^{III}(PQ_3)^+$ at −0.25 V in CH_2Cl_2 containing 3.5 equiv of TFA (Figure 9a), the Soret band shifts from 466 to 452 nm and the Q-band shifts from 654 to 600 nm as $Au^{III}(PQ_3H)^+$ is generated as a product of the one-electron reduction and following chemical reaction. Further reduction of $Au^{III}(PQ_3H)^+$ at −0.40 V in the acid containing CH_2Cl_2 solution gives a porphyrin product with a Soret band at 429 nm and a Q-band at 562 nm (Figure 9b). This spectrum is assigned to $Au^{III}(PQ_3H_2)^+$ and is almost identical to the spectrum of $Au^{III}(PQ)^+$ which has bands at 435 and 588 nm in CH_2Cl_2.[12] The reduction of $Au^{III}(PQ_3H_2)^+$ at −0.60 V (Figure 9c) leads to $Au^{III}(PQ_3H_3)^+$ as a final porphyrin product (λ = 409, 520, and 640 nm) and this is followed by another Au^{III}/Au^{II} process at −0.80 V (Figure 9d) to give the Au(II) product $Au^{II}(PQ_3H_3)$. The UV−visible spectrum of the fully protonated Au(II) porphyrin is characterized by a Soret band at 420 nm and resembles the spectrum of both $Au^{II}(P)$ (420 nm)[12] and $Au^{II}(PQ_4H_4)$ (419 nm) (see Figure 10). Finally the reduction of $Au^{II}(PQ_3H_3)$ at −1.40 V (Figure 9e) results in a decreased intensity Soret band, consistent with the formation of an Au(II) porphyrin π-anion radical under the given solution conditions.

UV−visible spectra obtained before and after the first five reductions of $Au^{III}(PQ_4)^+$ in CH_2Cl_2 containing 4.5 equiv of TFA are shown in Figure 10. The stepwise products of the first four reductions and coupled chemical reactions are represented as $Au^{III}(PQ_4H_x)$ where x = 1−4, and the prevailing reduction mechanism is shown in Scheme 3. The maximum Soret band intensity of the Au(III) porphyrins is stepwise blue-shifted from 483 nm for x = 0 (the unprotonated porphyrin) to 405 nm for x = 4 (the fully protonated Q_4H_4 derivative).

In summary, the electrochemical and spectroelectrochemical properties of $Au^{III}(PQ_3)^+$ and $Au^{III}(PQ_4)^+$ were examined in CH_2Cl_2 containing 0.1 M TBAP. Each porphyrin undergoes one metal-centered reduction to form the corresponding Au(II) porphyrin, and this reaction is followed by two porphyrin ring-centered reductions and one or two Q-centered reductions. Different electrochemical behavior is seen for $Au^{III}(PQ_3)^+$ and $Au^{III}(PQ_4)^+$ as compared to the related P, PQ, and QPQ derivatives. Negative shifts in reduction potentials are seen upon going from $Au^{III}(QPQ)^+$ to $Au^{III}(PQ_3)^+$ to $Au^{III}(PQ_4)^+$ while positive shifts are observed upon going from the P to PQ to QPQ derivatives under the same solution conditions. All of the Au(III) quinoxalinoporphyrins in the presence of TFA will undergo multiple Au^{III}/Au^{II} processes because of an internal

dx.doi.org/10.1021/ic302380z | Inorg. Chem. 2013, 52, 2474−2483

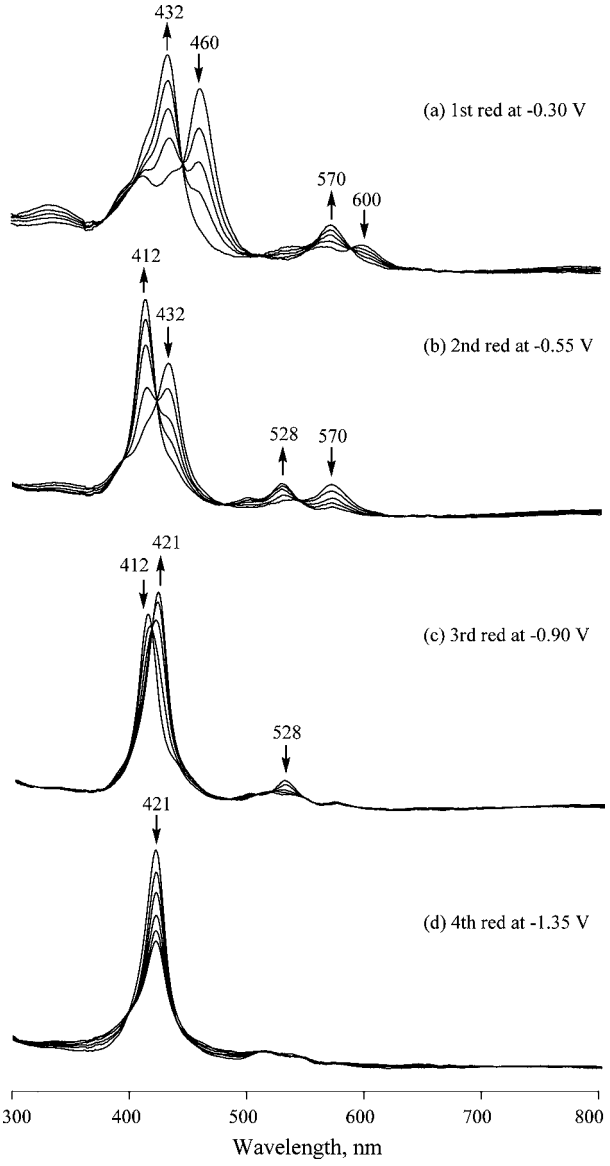

Figure 8. .Thin-layer UV−visible spectral changes of $Au(PQ_2)^+$ during reductions at (a) −0.30 (b) −0.55, (c) −0.90, and (d) −1.35 V in CH_2Cl_2 containing 0.1 M TBAP and 2.5 equiv of added TFA.

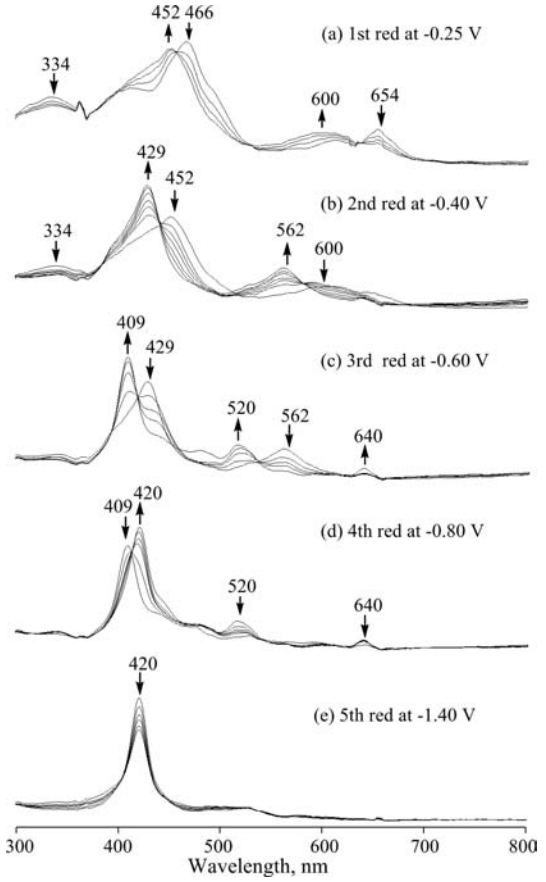

Figure 9. Thin-layer UV−visible spectral changes of $Au(PQ_3)^+$ during reductions at (a) −0.25, (b) −0.40, (c) −0.60, (d) −0.80, and (e) −1.40 V in CH_2Cl_2 containing 0.1 M TBAP and 3.5 equiv of added TFA.

electron transfer and protonation of the fused Q group(s) on the porphyrin macrocycle which regenerates a new Au(III) porphyrin with a reduced and protonated quinoxaline group. The number of multiple Au^{III}/Au^{II} reactions observed is one more than the number of Q groups on the compound. Thus, $Au^{III}(PQ)^+$ and $Au^{III}(QPQ)^+$ undergo two and three metal-centered reductions,[12] while $Au^{III}(PQ_3)^+$ undergoes four metal-centered reductions and $Au^{III}(PQ_4)^+$ exhibits five Au^{III}/Au^{II} processes in the presence of acid. The electrochemically initiated protonation of the Q-group changes not only the redox potentials of the compounds but also their UV−visible properties as well as the conjugation between the porphyrin ring and the quinoxaline units.

EXPERIMENTAL SECTION

Instrumentation. Cyclic voltammetry was carried out at 298 K using an EG&G Princeton Applied Research (PAR) 173 potentiostat/galvanostat. A homemade three-electrode cell was used for cyclic voltammetric measurements and consisted of a platinum button or glassy carbon working electrode, a platinum counter electrode and a homemade saturated calomel reference electrode (SCE). The SCE was separated from the bulk of the solution by a fritted glass bridge of low porosity which contained the solvent/supporting electrolyte mixture.

Thin-layer UV−visible spectroelectrochemical experiments were performed with a home-built thin-layer cell which has a light transparent platinum net working electrode. Potentials were applied and monitored with an EG&G PAR Model 173 potentiostat. Time-resolved UV−visible spectra were recorded with a Hewlett-Packard Model 8453 diode array spectrophotometer. High purity N_2 from Trigas was used to deoxygenate the solution and kept over the solution during each electrochemical and spectroelectrochemical experiment.

Chemicals. Dichloromethane (CH_2Cl_2) was obtained from Aldrich Co. and used as received for electrochemistry and spectroelectrochemistry experiments. Tetra-*n*-butylammonium perchlorate (TBAP) was purchased from Sigma Chemical or Fluka Chemika Co., recrystallized from ethyl alcohol, and dried under vacuum at 40 °C for at least one week prior to use.

Synthesis. Hexafluorophosphate{5,10,15,20-tetrakis(3,5-di-*tert*-butylphenyl)bisquinoxalino[2,3-*β*′:7,8-*β*″]porphyrinato}aurate(III), $Au^{III}(PQ_2)PF_6$ 5,10,15,20-Tetrakis(3,5-di-*tert*-butylphenyl) bisquinoxalino[2,3-*β*′:7,8-*β*″]porphyrin (41.0 mg, 0.0316 mmol), potassium tetrachloroaurate(III) (37.0 mg, 0.0979 mmol), and sodium acetate (61.0 mg, 0.744 mmol) were dissolved in a solution of toluene (12 mL) and glacial acetic acid (18 M, 12 mL). The reaction mixture was heated at reflux for 10 min. The mixture was then diluted in dichloromethane (30 mL) and washed with water (2 × 100 mL), sodium carbonate solution (10%, 2 × 100 mL), water (2 × 100 mL), dried over anhydrous sodium sulfate, filtered, and the filtrate evaporated to dryness. The residue was dissolved in chloroform (12

dx.doi.org/10.1021/ic302380z | Inorg. Chem. 2013, 52, 2474−2483

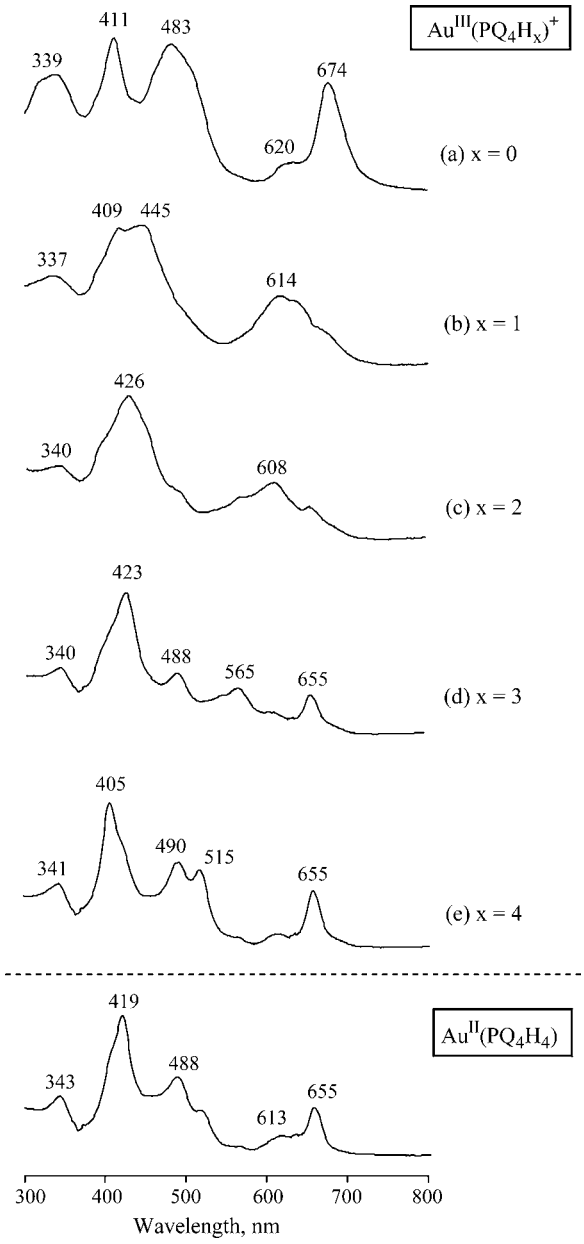

Figure 10. UV−visible spectra of $Au^{III}(PQ_4)^+$ and its stepwise reduction products in CH_2Cl_2 containing 0.1 M TBAP and 4.5 equiv of added TFA.

mL) and stirred with a saturated solution of potassium hexafluorophosphate (0.600 g, 0.326 mmol) in water (12 mL) for 18 h. The mixture was then diluted in chloroform (40 mL) and washed with water (2 × 200 mL) and dried over anhydrous sodium sulfate, filtered, and the filtrate evaporated to dryness. The mixture was then purified by column chromatography over silica (chloroform/methanol; 100:3). The polar green band was collected and the solvent removed. The product was redissolved in chloroform (10 mL) and stirred with a saturated solution of potassium hexafluorophosphate (0.702 g, 0.381 mmol) in water (10 mL) for 18 h. The mixture was then washed with water (2 × 200 mL) and dried over anhydrous sodium sulfate, filtered, and the filtrate evaporated to dryness. The green purple band was collected and evaporated to afford pure hexafluorophosphate-{5,10,15,20-tetrakis(3,5-di-*tert*-butylphenyl)bisquinoxalino[2,3-*β*′:7,8-*β*″]porphyrinato}aurate(III) (35.0 mg, 69%) as a black solid, mp >300 °C. Found: C, 65.28; H, 6.22; N, 6.74. $C_{88}H_{96}AuF_6N_8P$ requires C, 65.74; H, 6.02; N, 6.74%. (HR-MALDI-FTICR Found: $[M - PF_6]^+$ 1461.73991. $C_{88}H_{96}AuN_8$ requires 1461.74180). ν_{max} ($CHCl_3$): 3061 w, 2964 s, 2905 m, 2866 m, 1595 s, 1491 w, 1477 m, 1464 w, 1431 w, 1394 w, 1300 w, 1238 m, 1186 w, 1122 w, 955 w cm^{-1}. λ_{max} ($CHCl_3$) (log ε): 332 (4.61), 410 (4.77), 434sh (4.76), 460 (5.10), 561 (4.22), 597 (4.26) nm. ^1H NMR (400 MHz, $CDCl_3$): δ 1.45 (18 H, s, *t*-butyl H); 1.48 (36 H, s, *t*-butyl H); 1.53 (18 H, s, *t*-butyl H); 7.86 (2 H, d, *J* 1.8 Hz, H_o); 7.88−8.01 (15 H, m, quinoxaline H, H_o, H_p); 8.04 (2 H, d, *J* 1.8 Hz, H_o); 8.10 (1 H, t, *J* 1.8 Hz, H_p); 9.12 and 9.22 (4 H, ABq, *J* 5.1 Hz, *β*-pyrrolic H). ^{31}P NMR (162 MHz, $CDCl_3$): δ −146.33 (1 P, h, *J* 714 Hz, PF_6). ^{19}F NMR (282 MHz, $CDCl_3$): δ −75.13 (6 F, d, *J* 714 Hz, PF_6). Mass spectrum (ESI) (*m*/*z*): 1462.3 ($[M - PF_6]^+$ requires 1461.7).

Hexafluorophosphate{5,10,15,20-tetrakis(3,5-di-*tert*-butylphenyl)-trisquinoxalino[2,3-*β*′:7,8-*β*″:12,13-*β*‴]-porphyrinato}aurate(III), $Au^{III}(PQ_3)PF_6$ {5,10,15,20-Tetrakis(3,5-di-*tert*-butylphenyl)trisquinoxalino[2,3-*β*′:7,8-*β*″:12,13-*β*‴]porphyrin[22,23] (42.0 mg, 0.0306 mmol), potassium tetra-chloroaurate(III) (59.7 mg, 0.158 mmol) and sodium acetate (56.0 mg, 0.683 mmol) were dissolved in a solution of toluene (7 mL) and glacial acetic acid (18M, 7 mL). The reaction mixture was heated at reflux for 1 h. The mixture was then diluted in dichloromethane (30 mL) and washed with water (2 × 100 mL), sodium carbonate solution (10%, 100 mL), water (2 × 100 mL), dried over anhydrous sodium sulfate, filtered, and the filtrate evaporated to dryness. The residue was dissolved in chloroform (12 mL) and stirred with a saturated solution of potassium hexafluorophosphate (1.13g, 6.112 mmol) in water (12 mL) for 18 h. The mixture was then diluted in dichloromethane (40 mL) and washed with water (2 × 100 mL), dried over anhydrous sodium sulfate, filtered, and the filtrate evaporated to dryness. The mixture was then purified by column chromatography over silica (chloroform/methanol; 100:4). The polar green band was collected, and the solvent was removed to afford pure hexafluorophosphate{5,10,15, 20-tetrakis(3,5-di-*tert*-butylphenyl)trisquinoxalino[2,3-*β*′:7,8-*β*″:12,13-*β*‴]-porphyrinato}aurate(III) (50 mg, 96%) as a green solid, mp >300 °C. IR (*ν*, cm^{-1}, $CHCl_3$): 3060w, 2964s, 2905s, 2868m, 1595s, 1491w, 1477m, 1462w, 1393w, 1362s, 1302w, 1248m, 1234s, 1190m, 1161w, 999w. UV−vis (*λ*, nm, $CHCl_3$): 312sh (log *ε* 4.61), 335 (4.67), 400sh (4.66), 415 (4.67), 467 (4.90), 573sh (3.98), 613 (4.18), 653 (4.33). ^1H NMR (400 MHz, $CDCl_3$): δ 1.46 (36 H, s, *t*-butyl H); 1.48 (36 H, s, *t*-butyl H); 7.86 (4 H, d, *J* 1.7 Hz, H_o); 7.90 (4 H, d, *J* 1.8 Hz, H_o); 7.91−8.05 (14 H, m, quinoxaline H, H_p); 8.08 (2 H, t, *J* 1.8 Hz, H_p); 9.26 (2 H, s, *β*-pyrrolic H). ^{19}F NMR (282 MHz, $CDCl_3$): δ −70.35 (6 F, d, *J* 714 Hz, PF_6). MS (ESI): 1564.9 ($[M-PF_6]^+$ requires 1564.8). HR-MALDI-FTICR found: $[M-PF_6]^+$ 1563.76201 requires 1563.7630.

Hexafluorophosphate{5,10,15,20-tetrakis(3,5-di-*tert*-butylphenyl)-tetrakisquinoxalino[2,3-*β*′:7,8-*β*″:12,13-*β*‴:17,18-*β*⁗′]porphyrinato}-aurate(III), $Au^{III}(PQ_4)PF_6$ 5,10,15,20-tetrakis(3,5-di-*tert*-butylphenyl)tetrakisquinoxalino[2,3-*β*′:7,8-*β*″:12,13-*β*‴:17,18-*β*⁗′]-porphyrin[23] (36.7 mg, 0.0249 mmol), potassium tetrachloroaurate(III) (44.0 mg, 0.116 mmol), and sodium acetate (49.0 mg, 0.597 mmol) were dissolved in a solution of toluene (7 mL) and glacial acetic acid (18 M, 7 mL). The reaction mixture was heated at reflux for 15 min. The mixture was then diluted with dichloromethane (40 mL) and the organic phase washed with water (2 × 100 mL), sodium carbonate solution (10%, 100 mL), water (2 × 100 mL), dried over anhydrous sodium sulfate, filtered, and the filtrate evaporated to dryness. The residue was dissolved in chloroform (12 mL) and stirred with a saturated solution of potassium hexafluorophosphate (1.13 g, 6.11 mmol) in water (12 mL) for 18 h. The mixture was then diluted in dichloromethane (40 mL) and washed with water (2 × 200 mL), dried over anhydrous sodium sulfate, filtered, and the filtrate evaporated to dryness. The mixture was then purified by column chromatography over silica (chloroform/methanol; 100:4). The polar brown green band was collected, and the solvent revolved to afford pure hexafluorophosphate{5,10,15,20-tetrakis(3,5-di-*tert*-butylphenyl)-tetrakisquinoxalino-[2,3-*β*′:7,8-*β*″:12,13-*β*‴:17,18-*β*⁗′]porphyrin}-aurate(III) (44.0 mg, 98%) as a green solid, mp > 300 °C. IR (*ν*, cm^{-1}, $CHCl_3$): 3061w, 2964s, 2903m, 2866m, 1597m, 1560w, 1553w, 1514w, 1491m, 1477m, 1460w, 1435w, 1393w, 1362s, 1352m, 1335w, 1302w, 1258s, 1248s, 1236s, 1161s, 1128w, 1082m, 1043w. UV−vis (*λ*, nm, $CHCl_3$): 320sh (log *ε* 4.78), 340 (4.81), 410 (4.91), 482

dx.doi.org/10.1021/ic302380z | Inorg. Chem. 2013, 52, 2474−2483

(4.91), 621 (4.19), 675 (4.77). ^{1}H NMR (400 MHz, $CDCl_3$): δ 1.47 (72 H, s, *t*-butyl H); 7.88 (8 H, br s, H_o); 7.96−7.99 (8 H, m, quinoxaline H); 8.03−8.06 (8 H, m, quinoxaline H); 8.07 (4 H, br s, H_p). ^{19}F NMR (282 MHz, $CDCl_3$): δ −76.95 (6 F, d, *J* 715 Hz, PF_6). MS (ESI) 1667.1 ($[M\text{-}PF_6]^+$ requires 1666.9). (HR-MALDI-FTICR Found: $[M\text{-}PF_6]^+$ 1665.78766 requires 1665.78539).

■ ASSOCIATED CONTENT

Supporting Information

ESR spectra of singly reduced gold porphyrins in CH_2Cl_2 at 77 K. Plots of reduction potentials of $Au^{III}(PQ_n)PF_6$ in THF and pyridine containing 0.1 M TBAP vs the number of quinoxaline groups. Plots of reduction potentials of $Au^{II}(PQ_n)$ in CH_2Cl_2 containing 0.1 M TBAP with and without added TFA vs the number of quinoxaline groups. This material is available free of charge via the Internet at http://pubs.acs.org.

■ AUTHOR INFORMATION

Corresponding Author

*E-mail: zpou2003@yahoo.com (Z.O.), m.crossley@chem.usyd.edu.au (M.J.C.), kkadish@uh.edu (K.M.K.).

Notes

The authors declare no competing financial interest.

■ ACKNOWLEDGMENTS

This work was supported by grants from the Robert A. Welch Foundation (K.M.K., Grant E-680) and the Natural Science Foundation of China (Grant 21071067). Support was also provided by a Discovery Research Grant (DP0208776) from the Australian Research Council to M.J.C.

■ REFERENCES

(1) Kadish, K. M.; Van Caemelbecke, E.; Rotal, G. In *The Porphyrin Handbook*; Kadish, K. M., Smith, K. M., Guilard, R., Eds.; Academic Press: New York, 2000; Vol. *8*, pp 1−114.

(2) Kadish, K. M.; E, W.; Ou, Z.; Shao, J.; Sintic, P. J.; Ohkubo, K.; Fukuzumi, S.; Crossley, M. J. *Chem. Commun.* **2002**, 356−357.

(3) Ou, Z.; Kadish, K. M.; E, W.; Shao, J.; Sintic, P. J.; Ohkubo, K.; Fukuzumi, S.; Crossley, M. J. *Inorg. Chem.* **2004**, *43*, 2078−2086.

(4) Zhu, W.; Sintic, M.; Ou, Z.; Sintic, P. J.; McDonald, J. A.; Brotherhood, P. R.; Crossley, M. J.; Kadish, K. M. *Inorg. Chem.* **2010**, *49*, 1027−1038.

(5) Ohkubo, K.; Garcia, R.; Sintic, P. J.; Khoury, T.; Crossley, M. J.; Kadish, K. M.; Fukuzumi, S. *Chem.—Eur. J.* **2009**, *15*, 10493−10503.

(6) Sintic, P. J.; E, W.; Ou, Z.; Shao, J.; McDonald, J. A.; Cai, Z.; Kadish, K. M.; Crossley, M. J.; Reimers, J. R. *Phys. Chem. Chem. Phys.* **2008**, *10*, 515−527.

(7) Ou, Z.; E, W.; Zhu, W.; Thordarson, P.; Sintic, P. J.; Crossley, M. J.; Kadish, K. M. *Inorg. Chem.* **2007**, *46*, 10840−10849.

(8) Kadish, K. M.; E, W.; Sintic, P. J.; Ou, Z.; Shao, J.; Ohkubo, K.; Fukuzumi, S.; Govenlock, L. J.; McDonald, J. A.; Try, A. C.; Cai, Z.; Reimers, J. R.; Crossley, M. J. *J. Phys. Chem. B* **2007**, *111*, 8762−8774.

(9) Hutchison, J. A.; Sintic, P. J.; Crossley, M. J.; Nagamura, T.; Ghiggino, K. P. *Phys. Chem. Chem. Phys.* **2009**, *11*, 3478−3489.

(10) Armstrong, R. S.; Foran, G. J.; Hough, W. A.; D'Alessandro, D. M.; Lay, P. A.; Crossley, M. J. *Dalton Trans.* **2006**, *40*, 4805−4813.

(11) Fukuzumi, S.; Ohkubo, K.; Zhu, W.; Sintic, M.; Khoury, T.; Sintic, P. J.; E, W.; Ou, Z.; Crossley, M. J.; Kadish, K. M. *J. Am. Chem. Soc.* **2008**, *130*, 9451−9458.

(12) Ou, Z.; Zhu, W.; Fang, Y.; Sintic, P. J.; Khoury, T.; Crossley, M. J.; Kadish, K. M. *Inorg. Chem.* **2011**, *50*, 12802−12809.

(13) E, W.; Kadish, K. M.; Sintic, P.; Khoury, T.; Govenlock, L.; Ou, Z.; Shao, J.; Ohkubo, K.; Reimers, J.; Fukuzumi, S.; Crossley, M. *J. Phys. Chem. A* **2008**, *112*, 556−570.

(14) Ou, Z.; Zhu, W.; Sintic, P.; Fang, Y.; Crossley, M.; Kadish, K. M. *J. Porphyrins Phthalocyanines* **2012**, *16*, 5−6.

(15) Stintic, P.; E, W.; Ou, Z.; Shao, J.; Mcdonald, J.; Cai, Z.; Kadish, K. M. *Phys. Chem. Chem. Phys.* **2008**, *10*, 268−280.

(16) Ou, Z.; E, W.; Shao, J.; Burn, P.; Craig, S.; Robin, W.; Kadish, K. M.; Crossley, M. J. *J. Porphyrins Phthalocyanines* **2005**, *9*, 142−151.

(17) Crossley, M. J.; Sintic, P. J.; Walton, R.; Reimers, J. R. *Org. Biomol. Chem.* **2003**, *1*, 2777−2787.

(18) Kadish, K. M.; Li, J.; Van Caemelbecke, E.; Ou, Z.; Guo, N.; Autret, M.; D'Souza, F.; Tagliatesta, P. *Inorg. Chem.* **1997**, *36*, 6292−6298.

(19) D'Souza, F.; Zandler, M. E.; Tagliatesta, P.; Ou, Z.; Shao, J.; Van Caemelbecke, E.; Kadish, K. M. *Inorg. Chem.* **1998**, *37*, 4567−4572.

(20) Tagliatesta, P.; Li, J.; Autret, M.; Van Caemelbecke, E.; Villard, A.; D'Souza, F.; Kadish, K. M. *Inorg. Chem.* **1996**, *35*, 5570−5576.

(21) Kadish, K. M.; D'Souza, F.; Villard, A.; Autret, M.; Van Caemelbecke, E.; Bianco, P.; Antonini, A.; Tagliatesta, P. *Inorg. Chem.* **1994**, *33*, 5169−5170.

(22) Khoury, T.; Crossley, M. J. *New J. Chem.* **2009**, *33*, 1076−1086.

(23) Khoury, T.; Crossley, M. J. *Chem. Commun.* **2007**, *46*, 4851−4853.